NAVAL POSTGRADUATE SCHOOL

MONTEREY, CALIFORNIA

THESIS

SIMULATION OF RADIOWAVE PROPAGATION IN A DENSE URBAN ENVIRONMENT

by

Chris V. Chung

March 2007

Thesis Advisor:	David C. Jenn
Second Reader:	Donald Z. Wadsworth

Approved for public release, distribution is unlimited

THIS PAGE INTENTIONALLY LEFT BLANK

REPORT DOCUMENTATION PAGE			Form Approved OMB No. 0704-0188
Public reporting burden for this collection of information is estimated to average 1 hour per response, including the time for reviewing instruction, searching existing data sources, gathering and maintaining the data needed, and completing and reviewing the collection of information. Send comments regarding this burden estimate or any other aspect of this collection of information, including suggestions for reducing this burden, to Washington headquarters Services, Directorate for Information Operations and Reports, 1215 Jefferson Davis Highway, Suite 1204, Arlington, VA 22202-4302, and to the Office of Management and Budget, Paperwork Reduction Project (0704-0188) Washington DC 20503.			
1. AGENCY USE ONLY ***(Leave blank)***	**2. REPORT DATE** March 2007	**3. REPORT TYPE AND DATES COVERED** Master's Thesis	
4. TITLE AND SUBTITLE Simulation of Radiowave Propagation in a Dense Urban Environment		**5. FUNDING NUMBERS**	
6. AUTHOR(S) Chris V. Chung			
7. PERFORMING ORGANIZATION NAME(S) AND ADDRESS(ES) Naval Postgraduate School Monterey, CA 93943-5000		**8. PERFORMING ORGANIZATION REPORT NUMBER**	
9. SPONSORING /MONITORING AGENCY NAME(S) AND ADDRESS(ES) N/A		**10. SPONSORING/MONITORING AGENCY REPORT NUMBER**	
11. SUPPLEMENTARY NOTES The views expressed in this thesis are those of the author and do not reflect the official policy or position of the Department of Defense or the U.S. Government.			
12a. DISTRIBUTION / AVAILABILITY STATEMENT Approved for public release, distribution is unlimited		**12b. DISTRIBUTION CODE**	

13. ABSTRACT (maximum 200 words)

One objective of this thesis was to investigate the effect of details, such as the windows of high-rise buildings, on the radiowave propagation in the dense urban environment through modeling and simulations. If adding windows does not significantly change the signal distribution on average, it may not be necessary to build such a detailed model. Simulations are performed using several levels of detail and the results compared to estimate the impact of the fine details on the signal level.

A second issue is base station antenna coverage. The antenna gain, half power beamwidth (HPBW), location, and pointing angle should be chosen to give the maximum coverage over a specified sector. Simulations can be used to select the optimums set of base station properties. Specifically this research looks at the coverage from the two sectored antennas versus a single one over a quadrant.

14. SUBJECT TERMS Radiowave propagation, *Urbana wireless toolset.*			**15. NUMBER OF PAGES** 65
			16. PRICE CODE
17. SECURITY CLASSIFICATION OF REPORT Unclassified	**18. SECURITY CLASSIFICATION OF THIS PAGE** Unclassified	**19. SECURITY CLASSIFICATION OF ABSTRACT** Unclassified	**20. LIMITATION OF ABSTRACT** UL

NSN 7540-01-280-5500 Standard Form 298 (Rev. 2-89)
Prescribed by ANSI Std. 239-18

THIS PAGE INTENTIONALLY LEFT BLANK

Approved for public release, distribution is unlimited

SIMULATION OF RADIOWAVE PROPAGATION IN A DENSE URBAN ENVIRONMENT

Chris V. Chung
Civilian, Air Force Flight Test Center, Edwards AFB
B.S., California State University, Fresno, 1989

Submitted in partial fulfillment of the
requirements for the degree of

MASTER OF SCIENCE IN ELECTRICAL ENGINEERING

from the

NAVAL POSTGRADUATE SCHOOL

March 2007

Author: Chris V. Chung

Approved by: David C. Jenn
Thesis Advisor

Donald Z. Wadsworth
Second Reader

Jeffrey B. Knorr
Chairman, Department of Electrical and Computer Engineer

THIS PAGE INTENTIONALLY LEFT BLANK

ABSTRACT

One objective of this thesis was to investigate the effect of details, such as the windows of high-rise buildings, on the radiowave propagation in the dense urban environment through modeling and simulations. If adding windows does not significantly change the signal distribution on average, it may not be necessary to build such a detailed model. Simulations are performed using several levels of detail and the results compared to estimate the impact of the fine details on the signal level.

A second issue is base station antenna coverage. The antenna gain, half power beamwidth (HPBW), location, and pointing angle should be chosen to give the maximum coverage over a specified sector. Simulations can be used to select the optimum set of base station properties. Specifically this research looks at the coverage over a quadrant from the two sectored antennas versus a single one.

THIS PAGE INTENTIONALLY LEFT BLANK

TABLE OF CONTENTS

I. INTRODUCTION....1
A. BACKGROUND....1
B. OBJECTIVES....2
C. RELATED WORK....3
D. THESIS OUTLINE....4

II. RADIOWAVE PROPAGATION IN THE URBAN ENVIRONMENT....7
A. PHYSICS OF PROPAGATION....7
1. Electromagnetic Radiation....7
2. Relationship Between Spherical Waves and Plane Waves....9
B. RAY OPTICS....10
1. Geometric Optics....10
2. Geometric Theory of Diffraction....11
C. ANTENNA FUNDAMENTALS....12
1. Antenna Radiation Pattern....12
2. Directivity and Gain....13
3. Antenna Polarization....15
4. Free-Space Link Equation....16
D. THEORETICAL MODELS FOR URBAN PROPAGATION....17
1. The Diffracting Screens Model....17
2. The COST 231 Model....18
E. EMPIRICAL MODELS FOR URBAN PROPAGATION....19
1. The Okumura Signal Prediction Method....19
2. The Hata and Modified Hata Formulas....19
3. Propagation Near Buildings....20
F. SOFTWARE TOOLS....21
1. Rhinoceros CAD Software....21
2. Urbana Wireless Toolset....22
G. SIMULATION MODEL....23

III. URBANA SIMULATION RESULTS....25
A. SIMULATION MODELS AND PARAMETERS....25
B. SIMULATION RESULTS FOR BUILDING MATERIALS....30
C. SIMULATION RESULTS FOR ANTENNA PATTERNS....38

IV. CONCLUSIONS AND FUTURE WORK....41
A. SUMMARY....41
B. CONCLUSIONS....42
C. FUTURE WORK....42

LIST OF REFERENCES....45

INITIAL DISTRIBUTION LIST....47

THIS PAGE INTENTIONALLY LEFT BLANK

LIST OF FIGURES

Figure 1. Periodic structure of railings, French Quarter New Orleans (from [7]) 4
Figure 2. Repeated rows of railings and balconies on an apartment building, NYC (from [8]) 4
Figure 3. Spherical wave (from [11]) 10
Figure 4. Flux tube (from [11]) 11
Figure 5. Principle of ray tracing model 12
Figure 6. Vertical dipole pattern in three dimensions. 13
Figure 7. (a) Ideal vertical dipole, (b) H-plane (azimuth) radiation pattern, (c) E-plane (elevation) radiation (from [9]). 13
Figure 8. Antenna directivities (from [9]) 14
Figure 9. Transmitter-receiver configuration. 17
Figure 10. Ray diffraction roofline to street level (from [13]) 18
Figure 11. Two-ray path propagation model showing the breaking point (from [13]) 21
Figure 12. *Urbana Wireless Toolset* and auxiliary programs (from [12]) 22
Figure 13. Baseline model (a) complete view (b) detailed view 24
Figure 14. Test model (a) complete view (b) detailed view 24
Figure 15. Observation grid (blue area) in over head view 26
Figure 16. Complete model and observation grid three dimensional view 28
Figure 17. Close up view of Windows 28
Figure 18. Antenna 1 pattern 29
Figure 19. Antenna 2 pattern 29
Figure 20. Antenna 3 pattern 30
Figure 21. Signal difference between baseline and detailed models for antenna 1 and concrete buildings f = 850 MHz 33
Figure 22. Signal difference between baseline and detailed models for antenna 2 and concrete buildings f = 850 MHz 33
Figure 23. Signal difference between baseline and detailed models for antenna 3 and concrete buildings f = 850 MHz 33
Figure 24. Signal difference between baseline and detailed models for antenna 1 and concrete buildings f = 900 MHz 34
Figure 25. Signal difference between baseline and detailed models for antenna 2 and concrete buildings f = 900 MHz 34
Figure 26. Signal Difference between baseline and detailed models for antenna 3 and concrete buildings f = 900 MHz 34
Figure 27. Signal difference between baseline and detailed models for antenna 1 and PEC buildings f = 850 MHz 35
Figure 28. Signal difference between baseline and detailed models for antenna 2 and PEC buildings f = 850 MHz 35
Figure 29. Signal difference between baseline and detailed models for antenna 3 and PEC buildings f = 850 MHz 35
Figure 30. Signal difference between baseline and detailed models for antenna 1 and PEC buildings f = 900 MHz 36

Figure 31. Signal difference between baseline and detailed models for antenna 2 and PEC buildings $f = 900$ MHz....36
Figure 32. Signal difference between baseline and detailed models for antenna 3 and PEC buildings $f = 900$ MHz....36
Figure 33. Simulation of an entire area with antenna 3 (a) diffracted fields (b) reflected fields....37
Figure 34. Simulation of an entire area for total field with antenna 3 (incident, reflected, and diffracted fields)....37

LIST OF TABLES

Table 1. Transmitting antennas characteristics 26
Table 2. Simulation input parameters 26
Table 3. Properties of the Building materials 27
Table 4. Simulation results of the diffracted and reflected fields for concrete buildings 31
Table 5. Simulation results of the diffracted and reflected fields for PEC buildings 32
Table 6. Summarized simulation parameters 32
Table 7. Simulation results of the total fields for detailed model 38

THIS PAGE INTENTIONALLY LEFT BLANK

ACKNOWLEDGMENTS

I am very grateful to the Long-Term Full-Time Training program and Edwards AFB which have provided the means for this unique and rewarding educational opportunity. Also, I would also like to thank Professor Donald Z. Wadsworth for his valuable support as the second reader.

I would like to extend a very special thanks to my thesis advisor, Professor David C. Jenn. His patience, guidance, and dedication, which he has so graciously put forwards, have made possible this work, and many others like it.

I am most grateful to my wife, Chi, my daughters, Caitlynn, and Cydney for their endless love, support, encouragement, and understanding in completing my Master's Degree and this thesis.

THIS PAGE INTENTIONALLY LEFT BLANK

EXECUTIVE SUMMARY

Since the proliferation of wireless devices in the 1990s, the study of radio frequency (RF) propagation in the urban environment has received much attention. With the increased demand for products and services incorporating wireless technology, the need for research into the behavior of RF propagation in the urban environment has come to the forefront.

Cellular telephone service providers are installing base stations in urban environments at locations that will ensure optimum customer access. These locations can be determined by conducting a costly RF survey of the coverage provided by the proposed base station location. Surveys may involve the placement of a transmitter and antenna at some proposed location, and then field strength is measured at multiple points throughout the service volume. This approach to the identification of base station placement is not only costly, but time consuming as well.

Computer simulation offers an alternative approach to the identification of optimum antenna placement. A computational electromagnetic (CEM) code, such as the *Urbana Wireless Toolset*, can be used to predict the RF propagation in some specified urban region. The simulation approach is not only time-saving, but much less costly than the RF survey.

One objective of this thesis was to investigate the effect of details, such as the windows of high-rise buildings, on the radiowave propagation in the dense urban environment through modeling and simulations.

A second issue is base station antenna coverage. The antenna gain, half power beamwidth (HPBW), location, and pointing angle should be chosen to give the maximum coverage over a specified sector.

In this thesis, a group of city blocks roughly modeled after New York City Manhattan Island near Central Park was used for simulation. The buildings were adapted from an existing CAD model of the city downloaded from 3d Cadbrowser.com. Each building was then reshaped and resized to match the dimensions of the actual city blocks.

Based on computer simulations which include ray tracing augmented by edge diffraction, we conclude that adding windows does not significantly change the signal distribution, on average. Data analysis from simulations also indicated that varying frequency over the specified range would have little impact on the overall results.

This thesis also analyzed the case where two antennas were used in combination and compared to the performance when only one larger beamwidth antenna was used with higher transmit power. The simulations results indicated that there was no apparent difference in performance between these two cases studied.

I. INTRODUCTION

A. BACKGROUND

Since the proliferation of wireless devices in the 1990s, the study of radio frequency (RF) propagation in the urban environment has received much attention. With the increased demand for products and services incorporating wireless technology, the need for research into the behavior of RF propagation in the urban environment has come to the forefront.

Cellular telephone service providers are installing base stations in urban environments at locations that will ensure optimum customer access. These locations can be determined by conducting a costly RF survey of the coverage provided by the proposed base station location. Surveys may involve the placement of a transmitter and antenna at some proposed location, and then field strength is measured at multiple points throughout the service volume. This approach to the identification of base station placement is not only costly, but time consuming as well.

Computer simulation offers an alternative approach to the identification of optimum antenna placement. A computational electromagnetic (CEM) code, such as the *Urbana Wireless Toolset*, can be used to predict the RF propagation in some specified urban region. The simulation approach is not only time-saving, but much less costly than the RF survey.

A major consideration in selecting the simulation approach is whether it is sufficiently accurate. The underlying electromagnetic (EM) theory is well known so it is a question of how accurately the EM equations are implemented and solved. Because of the frequencies involved ($\geq$ 1 GHz) high frequency techniques are usually employed. It has always been assumed that building wall reflections and corner and roof edge diffractions are the dominant propagation mechanisms. If this is the case then very crude models of buildings would suffice and would make the simulation approach much more appealing. However, recent studies by Ghoraish [1] have shown that signal scattering from objects such as lampposts, traffic lights, signboards can be comparable to the wall

reflections. Calculation of signals scattered from trees [2] have been done and the results were published recently.

These seemingly minor details can have a significant effect on nearby observation points. However, these are not the only objects that contribute to the scattering of radiowaves in the urban environment. There are the fine building details: window frames, railings, stairs, etc. A recent paper [3] suggests that multiple diffractions from periodic grating structures like railing slats dominate at sizable distances from the structures. Further investigation and evaluation of different levels of detail in the urban models seems to be necessary.

B. OBJECTIVES

Over the years, there have been numerous studies of how radiowaves could be affected when propagating in an urban environment. Ray tracing is one of the methods that offer the potential for the greatest accuracy in complex environments and has been the focus of much research over recent years. Ray tracing includes the method of geometrical optics (GO) and the geometrical theory of diffraction (GTD). Ray tracing requires extremely accurate terrain and clutter databases and calculations can be computationally expensive due to the large number of rays that must be traced [4].

One objective of this thesis was to investigate the effect of details, such as the windows of high-rise buildings, on the radiowave propagation in the dense urban environment through modeling and simulations. If adding window and door frames does not significantly change the signal distribution on average, then it may not be necessary to build such a detailed model. Simulations are performed using several levels of detail and their results compared to estimate the impact of the fine details on the signal level.

A second issue is base station antenna coverage. The antenna gain, half power beamwidth (HPBW), location, and pointing angle should be chosen to give the maximum coverage over a specified sector. Simulations can be used to select the optimum set of base station properties. Specifically this research looks at the coverage over a quadrant from two slightly overlapping sectored antennas versus a single one with a larger HPBW.

A test model was used to simulate the effects of different material properties, antenna patterns, and frequency variation. The simulations also accounted for diffraction, which is particularly significant in outdoor urban propagation environments.

The simulation results predict the local mean power received at any given point on the observation grid. For each observation point, the vector sum of the multipath field can be computed. Data can then be presented graphically for quantitative evaluation or it also can be presented tabulated for more detailed examination.

C. RELATED WORK

Following are some recent studies that utilize the ray-tracing technique to model urban propagation.

In [5] three diversity techniques were investigated to assess their performance in an urban environment. They were spatial diversity, polarization diversity, and angle diversity. These techniques were simulated for a UAV platform operating over a small city. The urban model of single building material was used with limited detail of the building. The results indicated that angle diversity has the most significant improvement in received signal strength as compared to the other two techniques.

Pala [6] examined propagation for several frequencies. The results indicated that high frequencies suffer attenuation more rapidly in lossy buildings. Vertically polarized antennas generally give better results than horizontally polarized antennas.

Ghoraishi [1] identified objects such as signboards, traffic signs, etc. that contributed to the scattering of the waves in the urban environment. This paper concluded that scattering from these objects can be comparable to wall reflection and, in any case, it has a significant contribution to the non-line of sight (LoS) received waves. Any prediction of the urban propagation channel needs to carefully consider and evaluate these scattering effects. Finally, [4] examined the effect of architectural features such as repeated rows of railings on propagation. It found that double diffraction can be the dominant mechanism in determining the field decay at relatively large distances (~ 0.5 km) from the features when they are still in view. An example of such features is illustrated in Figure 1, which is a building in the French quarter in New Orleans. Similar

features appear on more modern buildings as shown in Figure 2, which is located adjacent to Central Park in New York City.

Figure 1. Periodic structure of railings, French Quarter New Orleans (from [7])

Figure 2. Repeated rows of railings and balconies on an apartment building, NYC (from [8])

D. THESIS OUTLINE

Chapter II presents concepts in electromagnetics that are relevant to the problem under consideration. They include propagation mechanisms and antenna fundamentals. Software tools such as the *Urbana Wireless Toolset,* and *Rhinoceros* Computer Aided Design (CAD) are also discussed in this section. A flowchart is presented to illustrate the steps involved in running the *Urbana* program.

Chapter III presents results from simulations and provides data analysis. Data is presented in both graphical and tabular formats. Graphical data are used to demonstrate the effect of the details of the building on the radiowave propagation. The tabular data format is used for comparison between the different model conditions and variations in the base station antenna coverage.

Chapter IV presents conclusions, suggestions for future research, and final remarks.

THIS PAGE INTENTIONALLY LEFT BLANK

II. RADIOWAVE PROPAGATION IN THE URBAN ENVIRONMENT

In this chapter, some concepts in electromagnetics that are relevant to radiowave propagation in the urban environment are discussed. Also discussed are some of the common models used for the prediction of signal strength. The *Urbana wireless toolset* and *Rhinoceros* Computer Aided Design (CAD) software are also described.

A. PHYSICS OF PROPAGATION

1. Electromagnetic Radiation

Electromagnetic radiation is generally described as a propagating wave in space with electric and magnetic field components. These components oscillate at right angles to each other and to the direction of propagation, and they are in phase with each other in free space.

Maxwell derived a wave form of the electric and magnetic equations, revealing the wavelike nature of electric and magnetic fields and their symmetry. According to these equations, a time-varying electric field generates a magnetic field and vice versa. Therefore, as an oscillating electric field generates an oscillating magnetic field, the magnetic field in turn generates an oscillating electric field, and so on. These oscillating fields together form an electromagnetic wave [9].

Modern electromagnetism is based on a set of four fundamental relations known as Maxwell's equations. Using phasor quantities with a $e^{j\omega t}$ time convention, Maxwell's equations have the form

$$\nabla \cdot \vec{D} = \rho_v \qquad \textbf{2 - 1}$$

$$\nabla \times \vec{E} = -j\omega\vec{B} \qquad \textbf{2 - 2}$$

$$\nabla \cdot \vec{B} = 0 \qquad \textbf{2 - 3}$$

$$\nabla \times \vec{H} = \vec{J} + j\omega\vec{D} \qquad \textbf{2 - 4}$$

where $\vec{E}$ and $\vec{D}$ are the electric field intensity and electric flux density, respectively. They are related by $\vec{D} = \varepsilon \vec{E}$, with ε being the permittivity of the material. The magnetic field intensity, $\vec{H}$, and magnetic flux density, $\vec{B}$, are interrelated by $\vec{B} = \mu \vec{H}$, with μ being the magnetic permeability of the material. The charge density per unit volume is ρ_v and the volume current density is $\vec{J}$ [9].

Maxwell's equations for a charge free medium can be used to obtain the wave equation for the electric field

$$\nabla^2 \vec{E} - \gamma^2 \vec{E} = 0 \qquad \textbf{2 - 5}$$

where $\gamma = \omega\sqrt{\mu\varepsilon}$ is the propagation constant and $\omega = 2\pi f$.

Two important solutions to the wave equation are plane waves and spherical waves. A plane wave has the general form

$$\vec{E}(\vec{R}) = \vec{E}_0 e^{-\vec{\gamma}\cdot\vec{R}} \qquad \textbf{2 - 6}$$

where $\vec{R} = \hat{x}x + \hat{y}y + \hat{z}z$ is a position vector to the point (x, y, z). The vector $\vec{E}_0$ determines the polarization of the plane wave. The vector propagation constant is

$$\vec{\gamma} = \gamma_x \hat{x} + \gamma_y \hat{y} + \gamma_z \hat{z} \qquad \textbf{2 - 7}$$

where the components are given by

$$\gamma_x = \omega\sqrt{\mu\varepsilon}\,\hat{\gamma}\cdot\hat{x} \qquad \textbf{2 - 8}$$

$$\gamma_y = \omega\sqrt{\mu\varepsilon}\,\hat{\gamma}\cdot\hat{y} \qquad \textbf{2 - 9}$$

$$\gamma_z = \omega\sqrt{\mu\varepsilon}\,\hat{\gamma}\cdot\hat{z}, \qquad \textbf{2 - 10}$$

and $\hat{\gamma}$ is a unit vector in the direction of the propagation.

Spherical waves originating at the origin have the form

$$\vec{E}(r) = (E_\theta \hat{\theta} + E_\phi \hat{\phi})\frac{e^{-\gamma r}}{r}. \qquad \textbf{2 - 11}$$

Both plane and spherical waves are transverse electromagnetic (TEM) waves. The magnetic field intensity is obtained from

$$\vec{H}(r) = \frac{\hat{\gamma} \times \vec{E}(r)}{\eta}. \qquad \textbf{2 - 12}$$

The impedance of the medium is $\eta = \sqrt{\frac{\mu}{\varepsilon}}$.

The properties of an electromagnetic wave, such as its phase velocity, u_p, and wavelength, λ, are governed by angular frequency, ω, and the three constitutive parameters of the medium: ε, μ, and σ, such that

$$u_p = \frac{1}{\sqrt{\mu\varepsilon}}, \qquad \textbf{2 - 13}$$

$$\lambda = \frac{u_p}{f}, \qquad \textbf{2 - 14}$$

$$\mu = \mu_0 \mu_r = \mu_0 (\mu_r' - j\mu_r''), \qquad \textbf{2 - 15}$$

$$\varepsilon = \varepsilon_0 \varepsilon_r = \varepsilon_0 (\varepsilon_r' - j\varepsilon_r'') = \varepsilon_0 \left(\varepsilon_r' - j\frac{\sigma}{\omega\varepsilon_0} \right). \qquad \textbf{2 - 16}$$

If the medium is lossless ($\sigma = 0$ and $\mu'' = 0$), the wave does not suffer any attenuation as it travels through the medium. However, when the wave is propagating through a lossy medium, ($\sigma > 0$ or $\mu'' \neq 0$), absorption occurs as the wave passes through. Depending on the material the losses can be due to induced polarization, magnetization, or ohmic loss.

2. Relationship Between Spherical Waves and Plane Waves

When energy is emitted by a source, such as an antenna, it expands outwardly from the source in the form of spherical waves, as depicted in Figure 3 for an observer in the far field. The spherical wave travels at the same speed in all directions and expands at the same rate. If an observer is located sufficiently far from the source ($R \to \infty$), the wavefront of the spherical wave appears approximately planar, as if it were part of a

uniform plane wave with uniform properties at all points in the plane tangent to the wavefront as shown in Figure 3 [9]. Therefore, even though pure plane waves do not exist, the plane wave approximation can be used to accurately model real-world problems.

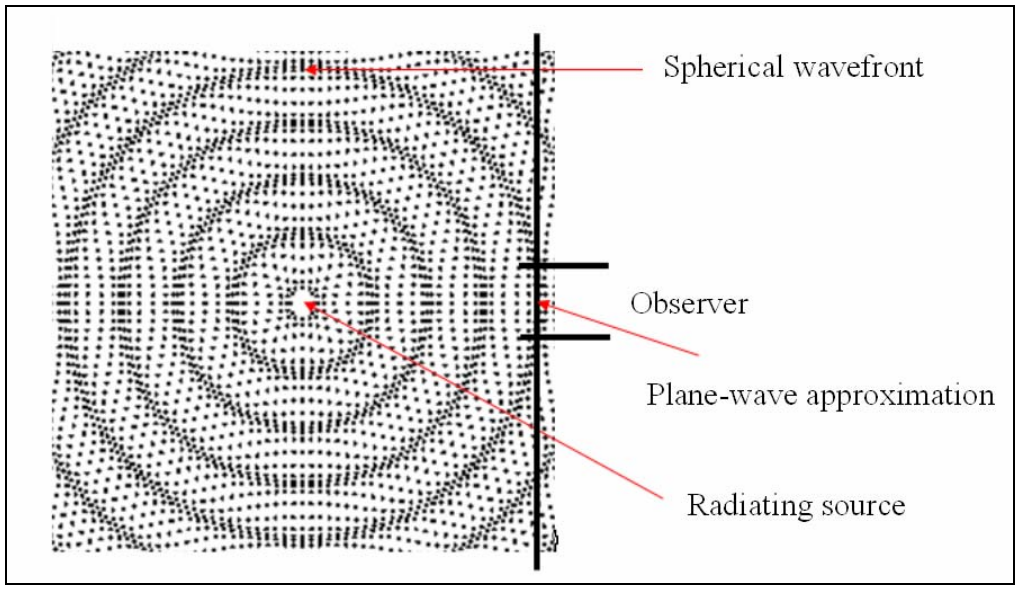

Figure 3. Spherical wave (from [11])

B. RAY OPTICS

Geometric optics (GO), also known as ray optics, represents an electromagnetic wave by a ray denoting the direction of travel of the wavefront. Neither the phase nor the polarization of the wave is accounted for explicitly in geometric optics. Thus, geometric optics is a ray approximation of physical optics [9].

1. Geometric Optics

In general, the GO method provides fairly accurate results whenever the size of the object illuminated by an electromagnetic wave is much larger than the wavelength, λ. GO also describes wave behavior upon reflection or refraction at an interface between two materials, based on the following assumptions [11]:

1. Wavefronts are locally plane and waves are TEM.
2. The wave direction is specified by the normal to the equiphase surface.

3. Rays travel in straight lines in a homogeneous medium.
4. Polarization is constant along a ray in an isotropic medium.
5. Power in flux tube is conserved as depicted in Figure 4.

$$\iint_{Area1} \vec{W} \cdot \vec{ds} = \iint_{Area2} \vec{W} \cdot \vec{ds} . \qquad \textbf{2 - 17}$$

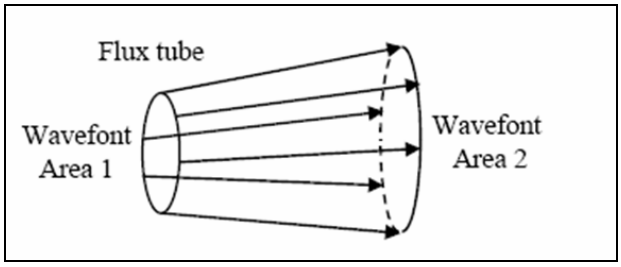

Figure 4. Flux tube (from [11])

6. The reflection of rays obeys Snell's law.
7. The reflected field is linearly related to the incident field at the reflected point by a reflection coefficient.

2. Geometric Theory of Diffraction

The geometric theory of diffraction (GTD) is a supplement to GO by the inclusion of diffraction. GTD eliminates some of the problems of GO, namely that GO does not account for the edge diffracted field. The total field at an observation point *P* can be found by the sum of GO and diffracted components [11]:

$$\vec{E}(P) = \vec{E}_{GO}(P) + \vec{E}_d(P) . \qquad \textbf{2 - 18}$$

Figure 5 illustrates how edge diffraction contributes to the field at an observation point *P*. The reflected and refracted rays comprise the GO part of the field. Multiple reflections are also possible although none are shown. Only single diffractions are shown; that is SAP and SBP. There are also multiple diffractions such as SABP. Finally, there are mixed terms such as reflected – diffracted that are less significant than the GO and GTD terms, and can be ignored.

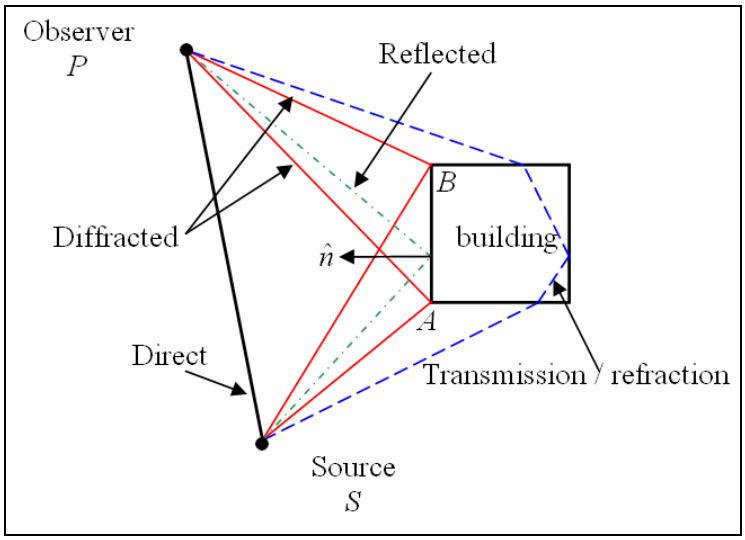

Figure 5. Principle of ray tracing model

C. ANTENNA FUNDAMENTALS

Antennas are treated as either transmitting or receiving as appropriate for the particular situation. In the receiving mode, antennas act to collect incoming waves and direct them to a common feed point where a transmission line is attached. Antennas have directional characteristics; that is, electromagnetic power density is radiated from a transmitting antenna with intensity that varies with angle around the antenna.

1. Antenna Radiation Pattern

The radiation pattern of an antenna gives the angular variation of radiation or reception at a fixed far field distance from the antenna. The antenna responds to an incoming wave from a given direction according to the pattern value in that direction. The normalized antenna pattern factor, $F(\theta,\phi)$, describes the shape of the radiation pattern in three-dimensional space. For a short dipole oriented along the z axis the normalized antenna pattern is

$$F(\theta,\phi) = \sin\theta\,. \qquad \textbf{2 - 19}$$

The complete three dimensional radiation pattern for the ideal dipole resembles a "doughnut" pattern as shown in Figure 6. The *E*-plane and *H*-plane patterns of the ideal dipole are shown in Figure 7 [9]. For a vertical dipole as shown, the pattern cut

transverse to the dipole axis is referred to as the azimuth pattern. The pattern cut that contains the dipole (z-axis) is referred to as the elevation pattern.

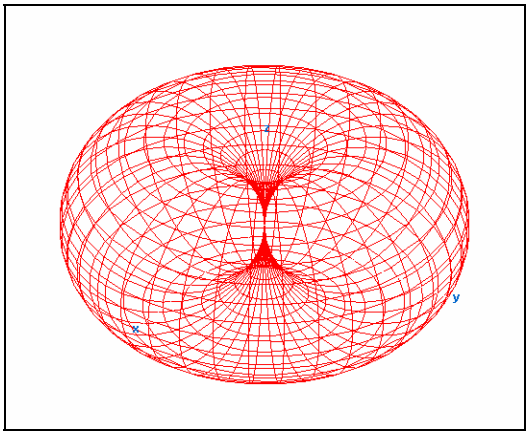

Figure 6. Vertical dipole pattern in three dimensions.

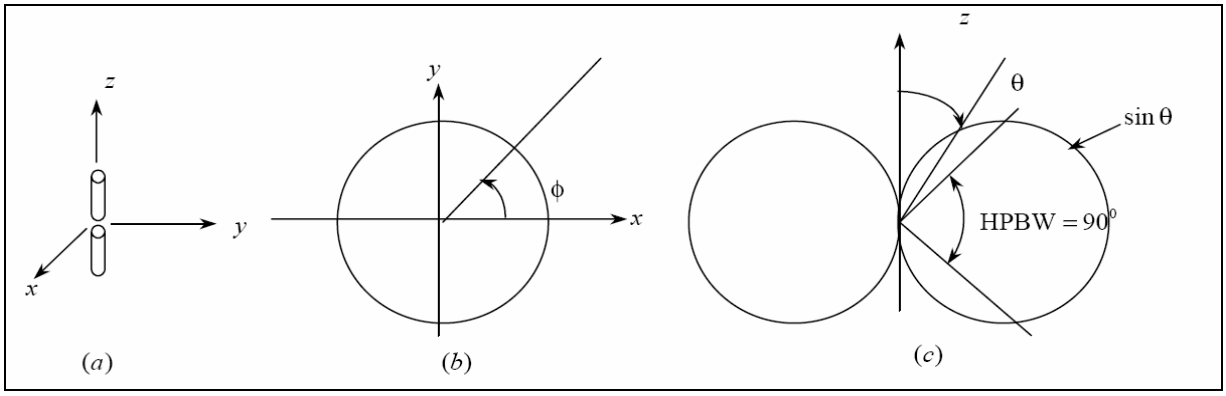

Figure 7. (a) Ideal vertical dipole, (b) H-plane (azimuth) radiation pattern, (c) E-plane (elevation) radiation (from [9]).

2. Directivity and Gain

The directivity of an antenna is defined as the ratio of the radiation intensity in a certain direction to the average radiation intensity, or

$$D = \frac{1}{\frac{1}{4\pi}\iint_{4\pi} |F(\theta,\phi)|^2 \, d\Omega} = \frac{4\pi}{\Omega_p} \qquad \textbf{2 - 20}$$

where Ω_p is referred to as the beam solid angle.

For an antenna with a single main lobe pointing in the *z*-direction as shown in Figure 8, Ω_p may be approximated as the product of the azimuth and elevation half power beamwidths ϕ_{HPBW} and θ_{HPBW} [9]

$$D \approx \frac{4\pi}{\theta_{HPBW}\phi_{HPBW}}. \qquad \textbf{2 - 21}$$

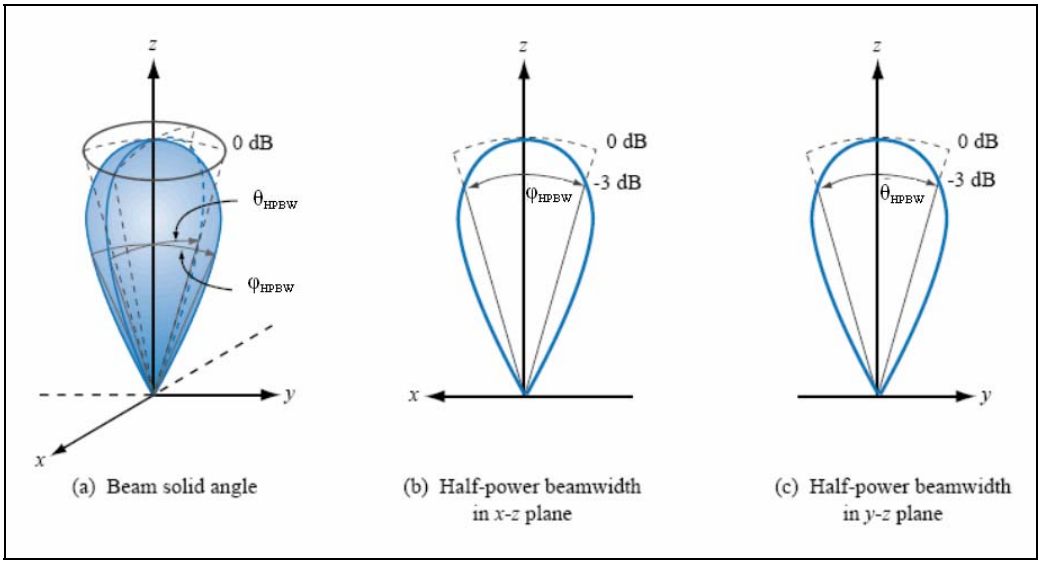

Figure 8. Antenna directivities (from [9]).

The gain, *G*, of an antenna is defined relative to the power into the antenna and thus includes loss. In practice, the gain of an antenna can be determined from its effective area, A_e, and the wavelength, λ, by

$$G = \xi D = \frac{4\pi A_e}{\lambda^2} \qquad \textbf{2 - 22}$$

where ξ is the radiation efficiency:

$$\xi = \frac{P_{radiated}}{P_{input}} \qquad (0 \le \xi \le 1). \qquad \textbf{2 - 23}$$

In this thesis, the antenna radiation is modeled as a $\cos^m \theta$ power pattern. The field pattern is of the form

$$\vec{E}(\theta,\phi) = \frac{e^{-jkr}}{r}(\hat{\theta}\cos^m\theta\cos\phi - \hat{\phi}\cos^m\theta\sin\phi), \qquad \theta \le \frac{\pi}{2}. \qquad \textbf{2 - 24}$$

Following is the sample calculation for the ERP. If the HPBW for each antenna is given then its corresponding gain can be computed from the specified HPBW. The HPBW is twice the half power angle

$$\theta_{HPBW} = 2\left\{\cos^{-1}\left(0.5^{\frac{1}{m}}\right)\right\}. \qquad \textbf{2 - 25}$$

From the HPBW it is possible to solve for *m*

$$m = \frac{\log(0.5)}{\log\left\{\cos\left(\frac{\theta_{HPWB}}{2}\right)\right\}}. \qquad \textbf{2 - 26}$$

For $\theta_{HPBW} = 55\,\text{deg}$, $m = 5.78$ and $\theta_{HPBW} = 110\,\text{deg}$, $m = 1.247$.

The directivity is [10]

$$D = 2(m+1) \qquad \textbf{2 - 27}$$

and the ERP for a lossless antenna ($G = D$) is

$$ERP = P_t G. \qquad \textbf{2 - 28}$$

3. Antenna Polarization

The energy radiated by any antenna is contained in a transverse electromagnetic wave that is comprised of electric and magnetic fields. For plane and spherical waves these fields are always orthogonal to one another and orthogonal to the direction of propagation. The electric field of the electromagnetic wave is used to describe its polarization and hence, the polarization of the antenna. In general, all polarizations fall under the general case of elliptically polarized. In this general case, the total electric field of the wave is comprised of two linear components, which are orthogonal to one another. Each of these components has a different magnitude and phase [9]. At any fixed point along the direction of propagation, the total electric field would trace out an ellipse as a function of time.

The two limiting cases of elliptical polarization are circular and linear. A circularly polarized electromagnetic wave is comprised of two linearly polarized electric field components that are orthogonal, have equal amplitude, and are 90 degrees out of phase. In this case, the polarization ellipse traced by the wave is a circle. Depending upon the direction of rotation of the electric field vector, the wave will be left-hand circularly polarized or right-hand circularly polarized. The phase relationship between the two orthogonal components, +90 degrees or –90 degrees, determines the direction of rotation. A linearly polarized electromagnetic wave is comprised of a single electric field component, and the polarization ellipse traced by the wave is a straight line [9]. Most commercial wireless systems are designed to operate with linear polarization, usually vertical with respect to the ground.

4. Free-Space Link Equation

The two antennas shown in Figure 9 are part of a free-space communication link, with the separation between the antennas, R, being large enough for each antenna to be in the far-field region of the other [13]. The transmitting and receiving antennas have effective areas A_t and A_r and radiation efficiencies, ξ_t and ξ_r, respectively. The antenna gains are related to their effective areas by Equation 2-22. The received signal power in free space can be expressed by the Friis transmission equation as follows:

$$P_r = \frac{P_t G_t G_r \lambda^2}{(4\pi R)^2}. \qquad \textbf{2 - 29}$$

Free space path loss is the spreading loss in signal between two isotropic antennas ($G_t = G_r = 1$), and it can be expressed as:

$$L_{fs} = \frac{P_r}{P_t} = \frac{\lambda^2}{(4\pi R)^2}. \qquad \textbf{2 - 30}$$

In urban propagation applications it is common to use d in place of R for distance from the transmitter.

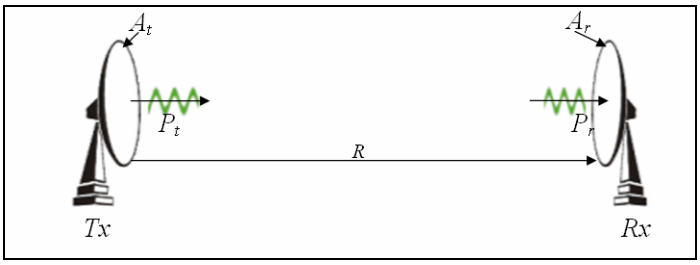

Figure 9. Transmitter-receiver configuration.

D. THEORETICAL MODELS FOR URBAN PROPAGATION

The urban and suburban propagation problems are complicated because the fields in the immediate vicinity of the portable or mobile radio are a superposition of localized multipath scattering. The signal strength varies from peak levels of a few decibels above the mean or median level to tens of decibels below the peaks in deep fades. Consequently, we often rely on a statistical description of the signal levels in the vicinity of the observer that states the local average and a description of the variation. There are many excellent models available for evaluation, however, only two models are considered: the diffracting screens model and the COST 231 model.

1. The Diffracting Screens Model

The urban propagation environment is complex and varied from one city to another, and even within a city. Simple approximations for the environment that are computationally efficient and accurate for a wide range of problems are desired.

The Walfisch-Bertoni [14] model is used widely for predicting the average path loss for mobile systems in urban areas. The model assumes that the street grid in a typical city organizes buildings into rows that are nearly parallel and that an idealized representation for the urban environment would be as shown in Figure 10, where the precise height and spacing of the buildings have been ignored and the profile is characterized by just two parameters: the mean building spacing s, and the mean building height b. The transmitting antenna is positioned at height H_b above ground level and the receiver antenna is positioned at H_m relative to the ground [13]. With this simple representation, the average path loss from the transmitter to the receiver is the sum of free

space wavefront spreading, multiple forward-diffraction past the rows of buildings and diffraction over the final rooftop down to the receiver [14].

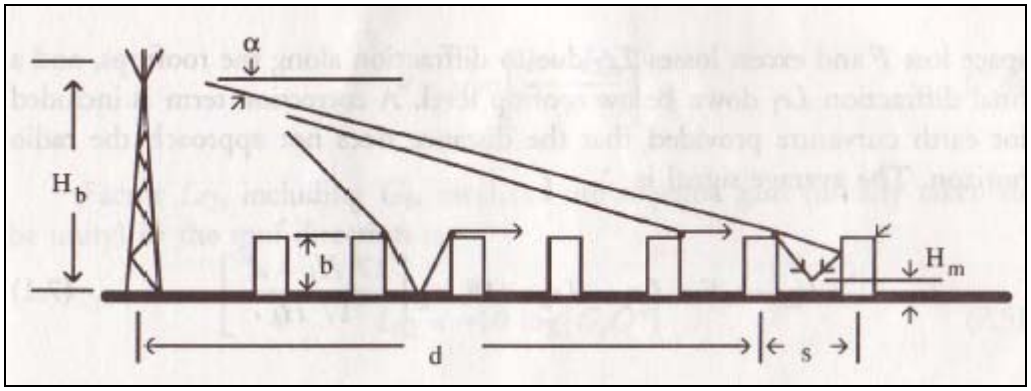

Figure 10. Ray diffraction roofline to street level (from [13])

The average excess loss above free space path loss, L_{ave-ex} predicted by the Walfisch-Bertoni model can be written as the summation of two independent terms: the multiple diffraction loss as the field propagates past the rows of buildings, L_{md} , and the diffraction loss from the last rooftop to the receiver, L_{rtr}

$$L_{ave-ex} = L_{md} + L_{rtr} . \qquad \textbf{2 - 31}$$

2. The COST 231 Model

The European Research Committee COST 231 created an urban propagation model based on the work of Walfisch and Bertoni and Ikegami [13]. The basic COST 231 model uses Walfisch-Bertoni results to calculate urban environment propagation prediction along with Ikegami's correction functions for taking into account the street orientation. The model was applied to the 800 MHz to 1.8 GHz bands and tested in the German cities Mannheim and Darmstadt. The street orientation influence was found to be minimal while it was found to require considerable improvements when the antenna was at or below rooftop level. The accuracy of the COST-231 model is best for antenna heights much greater than the building heights, and deteriorates when the height of the antenna is less than the height of the buildings [15]. The model becomes inaccurate when the terrain topography is non-flat or if the coating material of the land is inhomogeneous.

E. EMPIRICAL MODELS FOR URBAN PROPAGATION

Many empirical models have been developed over the years to overcome some of the limitations and assumptions presented by the theoretical models. The empirical models are based on measured data from which curve-fitted equations are obtained to model propagation in areas of definable urbanization. Often, empirical models are city-specific and are tied to urban land use maps. Following are examples of a few empirical models that are available [13].

1. The Okumura Signal Prediction Method

The experiment that Okumura [13] carried out was to measure the signal strengths in the vicinity of the city, Tokyo, over a wide range of frequencies, several fixed-site antenna heights, several mobile antenna heights, and over various irregular terrains and environmental clutter conditions. A set of curves relating field strength versus distance for a range of fixed-site heights at several frequencies was generated. Various behaviors in several environments, including the distance dependence of field strength in urban areas, and urban versus suburban differences were then extracted from these curves [13].

2. The Hata and Modified Hata Formulas

The Hata empirical model uses a propagation equation split into two terms: a term that has a logarithmic dependence on distance and a term that is independent of distance. The Hata model also includes adjustments to the basic equation to account for urban, suburban, and open area propagation losses [16]. The Hata equation for propagation loss in an urban area is given by:

$$L_p = 69.55 + 26.16\log_{10}(f) - 13.82\log_{10}(h_b) + [44.9 - 6.55\log_{10}(h_b)]\log_{10}(d) + a_x(h_m) \qquad \textbf{2 - 32}$$

where f is frequency in MHz, d is distance in kilometers, and h_b is the base station height in meters. A mobile height correction function, $a_x(h_m)$, is applied for mobile antenna heights. In a medium city, Hata's mobile height correction takes the form

$$a_m(h_m) = [0.7 - 1.12\log_{10}(f)]h_m + 1.56\log_{10}(f) - 0.8 \qquad \textbf{2 - 33}$$

while in a large city, at 200 MHz and below,

$$a_2(h_m) = 1.1 - 8.29\log_{10}^2[1.54h_m] \qquad \textbf{2 - 34}$$

while in a large city, at 400 MHz and below,

$$a_4(h_m) = 4.97 - 3.2\log_{10}^2[11.75h_m]. \qquad \textbf{2 - 35}$$

3. Propagation Near Buildings

Radiowave propagating in the urban environment can encounter additional losses due to the interference from nearby cells where the same frequency is reused. For short distances, there is a breakpoint beyond which the propagation law has increased losses with distance [13]. The following equation 2-36 can be used to explain the breakpoint

$$P_{2-ray} = \left| \frac{\sin\left[k\frac{2H_1H_2}{d}\right]}{2kd} + \frac{1}{(kXd)^2} \right|^2 \qquad \textbf{2 - 36}$$

where for vertical polarization X is

$$X = \frac{\sqrt{\varepsilon_g - \cos^2(\theta)}}{\varepsilon_g} \qquad \textbf{2 - 37}$$

for horizontal polarization X is

$$X = \sqrt{\varepsilon_g - \cos^2(\theta)} \qquad \textbf{2 - 38}$$

and:

θ is the incident angle,

ε_g is the dielectric constant of the ground,

H_1 is the transmitter's antenna height,

H_2 is the receiver's antenna height,

d is the distance between antennas,

k is the wave number.

At short distances, power falls off proportional to d^2. However, for longer distances, the signal strength is falling off at an d^4 rate. The breakpoint occurs at the rate's transition points from d^2 to d^4. Figure 11 demonstrates the two-ray path model where H_1 = 4 m, H_2 = 1.6 m, and frequency = 1.9 GHz. The breakpoint occurs at a distance of about 160 m for both the vertical and horizontal polarization [13].

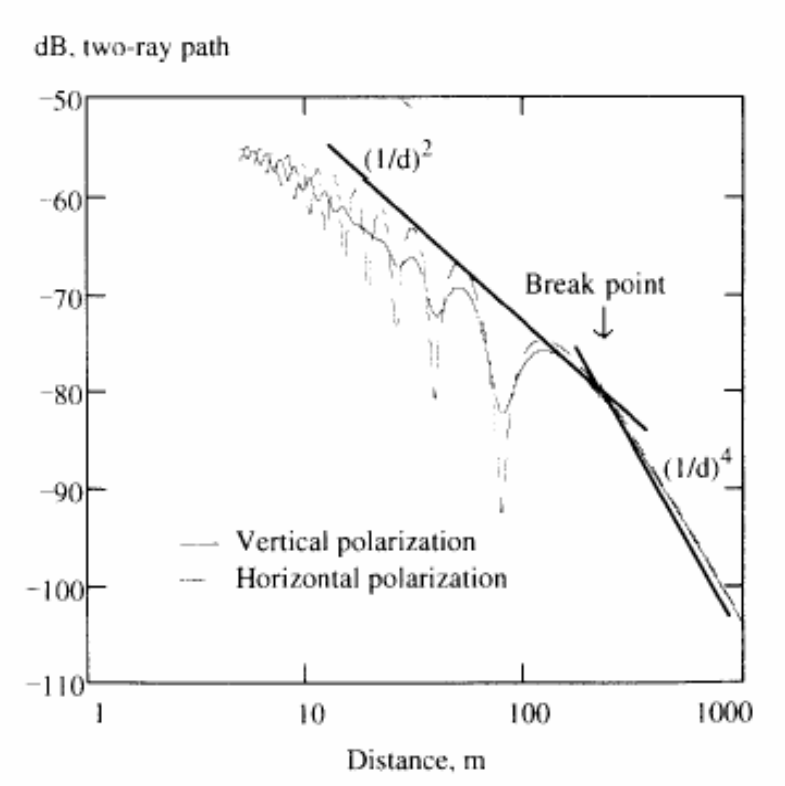

Figure 11. Two-ray path propagation model showing the breaking point (from [13])

F. SOFTWARE TOOLS

1. Rhinoceros CAD Software

Rhinoceros CAD for Windows platforms is a software package that can be used to draw and manipulate the geometry. For eventual use by *Urban* the file must be saved in 3-dimensional studio format (*.3ds). Since *Urbana* will read only a facet file format, the 3ds format files must first be converted to facet file format through the use of *Menelaus* tools. The next step is to extract edges from the facet file utilizing *Menelaus*

tools. Figure 12 shows the top level procedure in flow chart format to obtain the geometry input file, preparing an *Urbana* input file and post-processing using *Iurbana*.

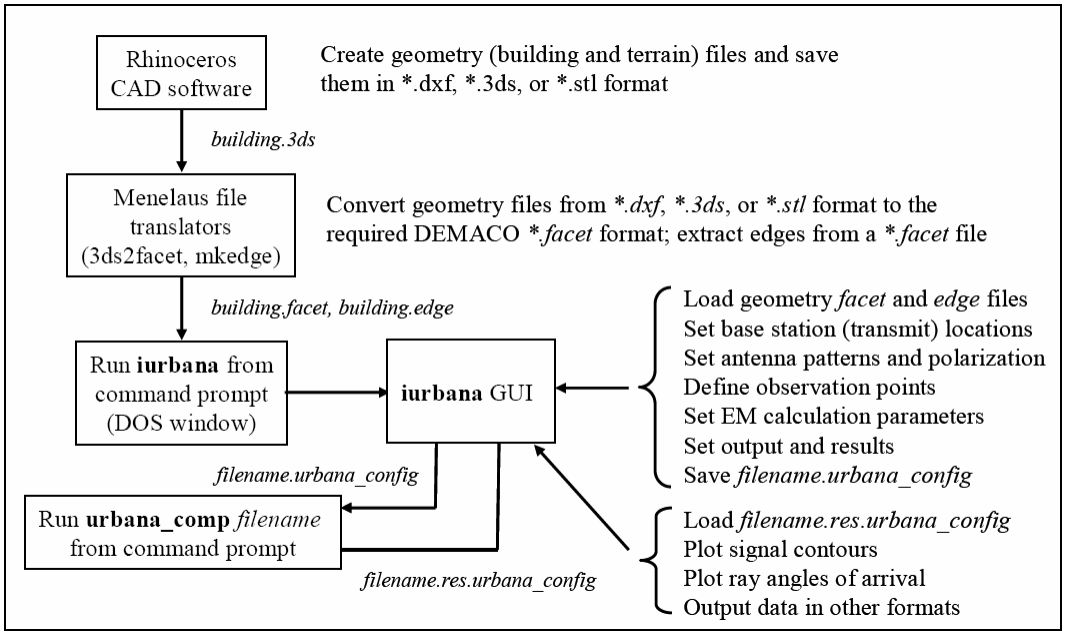

Figure 12. *Urbana Wireless Toolset* and auxiliary programs (from [12])

The *Urbana GUI* can present these results in graphic format or it can also export for plotting and analysis using *Matlab*. One way to determine if there is any impact due to windows is to calculate the difference in the electric field between a plain baseline model and detailed test model. *Matlab* software can also be used to determine the average, standard deviation, and maximum field strength at each point in the observation grid. These statistics are not normally provided by *Urbana.*

2. Urbana Wireless Toolset

The *Urbana Wireless Toolkit* is a computational electromagnetic tool for simulating wireless propagation in complex environments. The ray-tracing engine of the toolset is coupled with proprietary algorithms to implement physical optics, geometrical optics, and diffraction physics in producing a three-dimensional (3-D) simulation.

The ray-tracing process predicts the local mean power received at a given point at *x*, *y*, and *z*. For each point the vector sum of multipath power is computed. The calculations also include the effects of frequency, polarization, material properties, and

varying antenna patterns. If desired, the model can include the effects of ray diffraction. The following list is the key input parameters for *Urbana* simulation software:

1. Building facet and edge files.
2. User defined building materials.
3. Antenna patterns, placement, strength, frequency, and polarization.
4. Observation grid.

This toolkit contains two primary parts: *Urbana_comp* and *Iurbana*. *Urbana_comp* is the stand-alone back-end application to perform the simulation and post-processing. In addition to executing the simulation jobs, its primary value is that it allows batch job processing without the need for a GUI interface to launch each job. There are two additional applications, *Urbana* and *Urbana_rp,* which are controlled by *Urbana_comp* and are transparent to the user. These applications run the analysis calculations when provided with data from *Urbana_comp* [17].

G. SIMULATION MODEL

In this thesis, a group of city blocks roughly modeled after New York City Manhattan Island near Central Park was used for simulation. The buildings were adapted from an existing CAD model of the city downloaded from 3d Cadbrowser.com. Each building was then reshaped and resized to match the dimensions of the actual city blocks. The city model occupies an area of about 600 m by 500 m. The tallest building is at a height of 118 m. There are 24 separate city blocks that made up the simulation area.

In order to determine if windows would have any significant impact on the radiowave propagation, two models were built for comparison. The two models were identical in size, number of buildings, and building materials. Only one of these models has windows on two blocks of buildings and is referred to as the detailed or test model. The other model is used as reference and referred to as the baseline model. Figures 13 and 14 show the baseline model and test model respectively. Windows have been added to two blocks of buildings. The number was limited by the amount of computer memory.

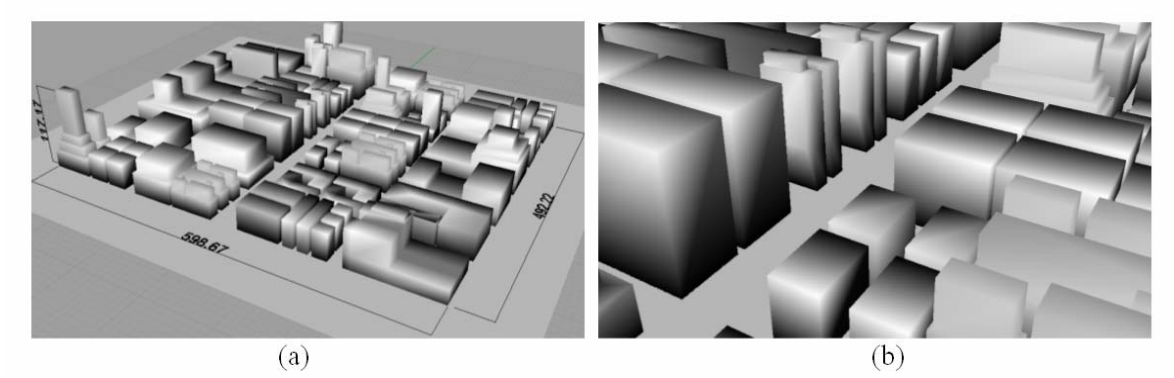

(a) (b)

Figure 13. Baseline model (a) complete view (b) detailed view

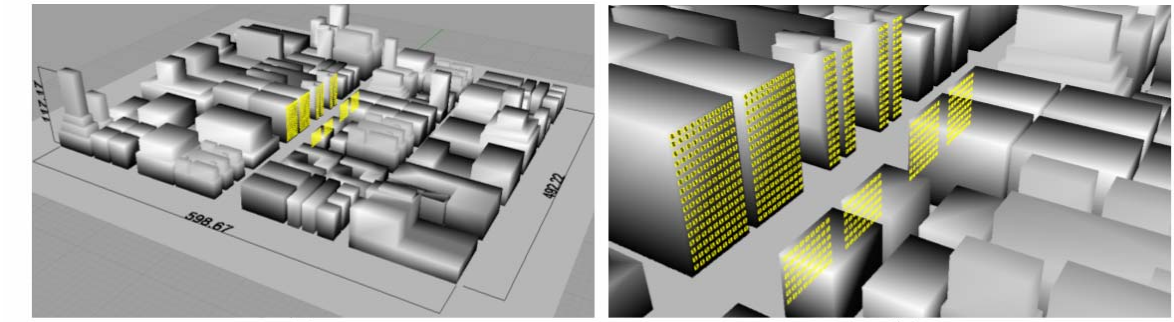

(a) (b)

Figure 14. Test model (a) complete view (b) detailed view

This chapter discussed theory and concepts relevant to the study of RF propagation in the urban environment. The next chapter presents the results of some simulations of RF propagation in a modeled urban environment. A few city blocks of Manhattan Island in NYC were modeled to study the RF propagation in this environment.

III. URBANA SIMULATION RESULTS

The previous chapter discussed concepts that were relevant to the study of radiowave propagation in the urban environment. This chapter will present the results of computer simulations that were conducted to satisfy two objectives:

Objective 1 is to investigate the effect of details, such as the windows of high-rise buildings, on the radiowave propagation.

Objective 2 is to illustrate how the base station antenna pattern affects coverage.

This chapter begins with an explanation of the parameters used in the set up of simulations and follows with presentation of the data generated from these simulations.

A. SIMULATION MODELS AND PARAMETERS

A group of city blocks modeled after Manhattan Island in NYC was used for this simulation. These models were previously discussed in Chapter II. NYC was chosen because it is a good example of a dense urban environment. Table 1 shows the transmitting characteristics of the antennas. Table 2 shows the input parameters for the simulations. The observation grids were set to an area of interest where buildings with windows are located. An observation grid is a region within the NYC model and it be defined in *Urbana* prior to the simulation. The height of the observation area and the resolution of each cell also have to be predefined. Figure 15 depicts the observation grid for this simulation, and it is highlighted in blue. Figure 16 shows the location of the antenna. Figure 17 shows a close up view of windows.

The transmit antenna patterns and the corresponding coverage areas are shown in Figures 18, 19, and 20. The antenna location is at the top of the tallest building at the corner of the model. Antennas 1 and 2 together provide complete coverage; antenna 3 by itself provides complete coverage. The z axis of the antenna (see Figure 8) is pointing downward slightly to give approximately uniform coverage. Before the antenna is tilted the polarization is vertical (z-directed electric field in Figure 8). Because the tilt angle is small the resulting polarization is very nearly vertical. The antenna pattern surface mesh in the figures is sized for viewing, and the intersection with the ground does not

necessarily represent the coverage area. The calculation of the antenna parameters is discussed in Section C.

Table 1. Transmitting antennas characteristics

Antenna	HPBW (deg)	Transmitting Power (W)	Antenna Gain (dBi)
1	55	1	13.3
2	55	1	13.3
3	110	3	4.8

Table 2. Simulation input parameters

Input Parameter	Input Values
Observation height	2 m
Grid cell resolution	0.5 x 0.5 m
Frequency 1	850 MHz
Frequency 2	900 MHz
GO Ray-bounces	5
Diffraction	single

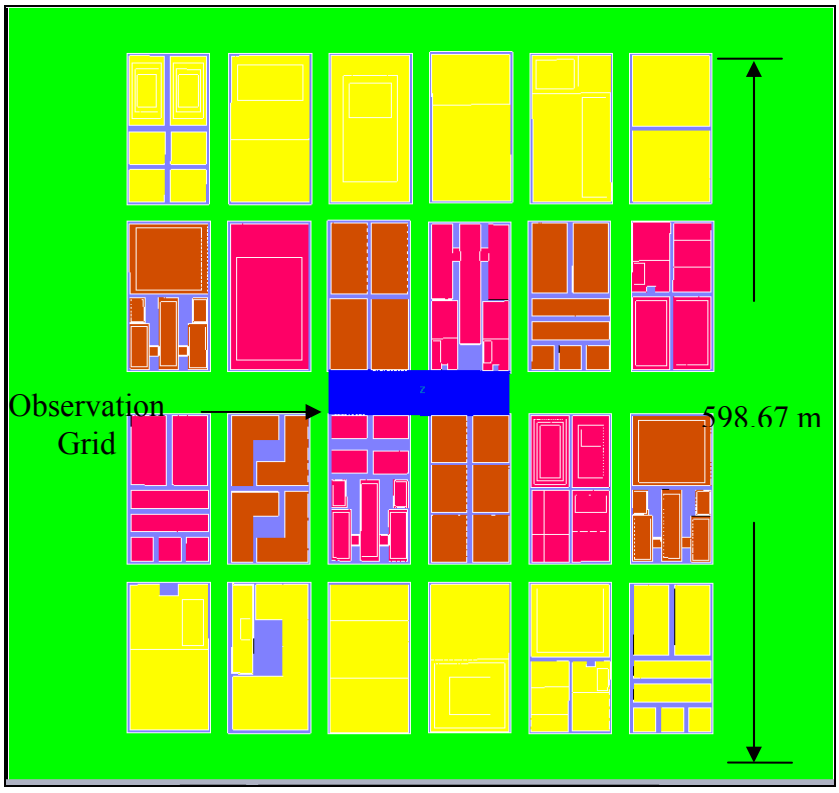

Figure 15. Observation grid (blue area) in over head view

Typical cell phone parameters were used for these simulations. Frequencies of 850 MHz and 900 MHz were chosen. These frequencies are 50 MHz apart, which is a typical bandwidth for wireless modulations.

In order to investigate the effect of materials on propagation, two separate models were built. One of the models was built with all PEC material, and the other model was built with a more realistic building material, such as concrete. Instead of cutting holes in buildings for windows, radar absorbing material (RAM) was used behind the glass windows to simulate the effect of radiowaves propagating through the windows and thus not reflected back out. This approximation eliminates the need to go back to *Rhino* and cut window openings in all of the buildings, which is a time consuming task. The material of the ground plane is the same as for all buildings in the model. The same thickness value is used for all building walls and ground plane. Table 3 summarizes the materials and their properties.

Table 3. Properties of the Building materials

Material	**Permeability**		**Permittivity**		**Thickness (cm)**
	μ'	μ''	ε'	ε''	
PEC	1	0	1	0	300
CONCRETE	10.2	0.5	1	0	300
GLASS	3.8	0	1	0	0.35
RAM	10	100	10	100	10

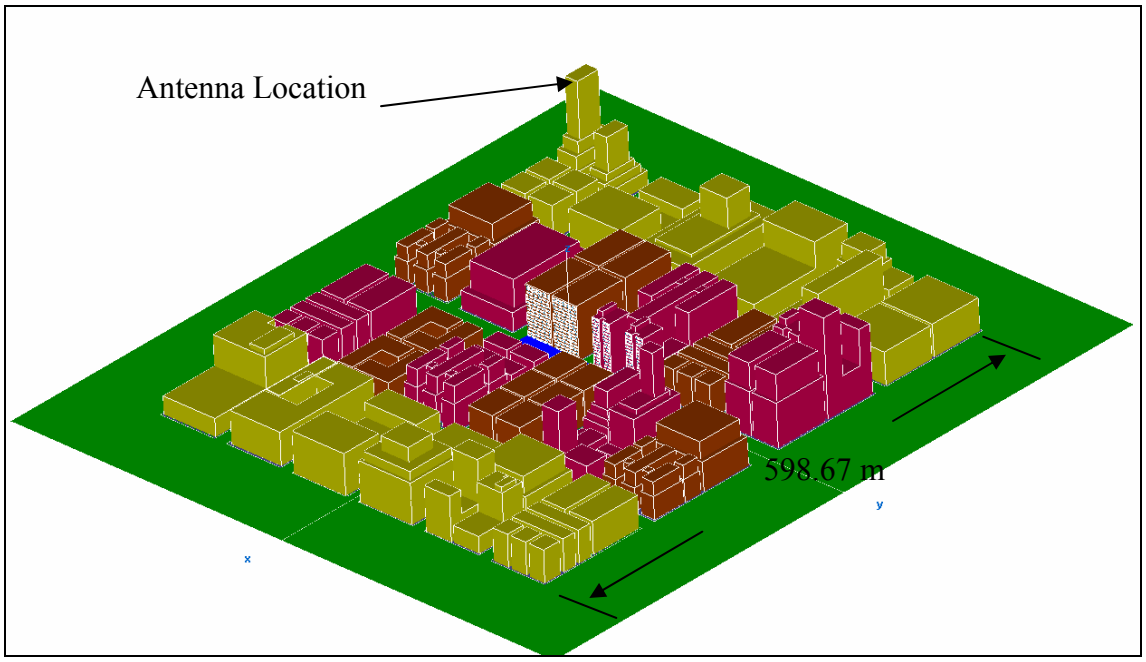

Figure 16. Complete model and observation grid three dimensional view

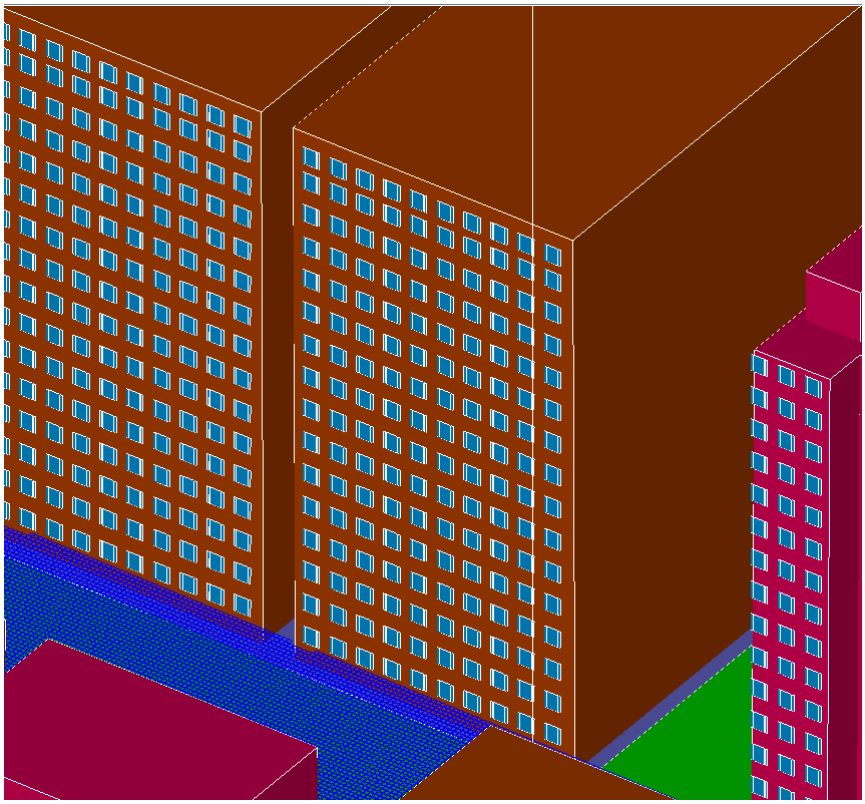

Figure 17. Close up view of Windows

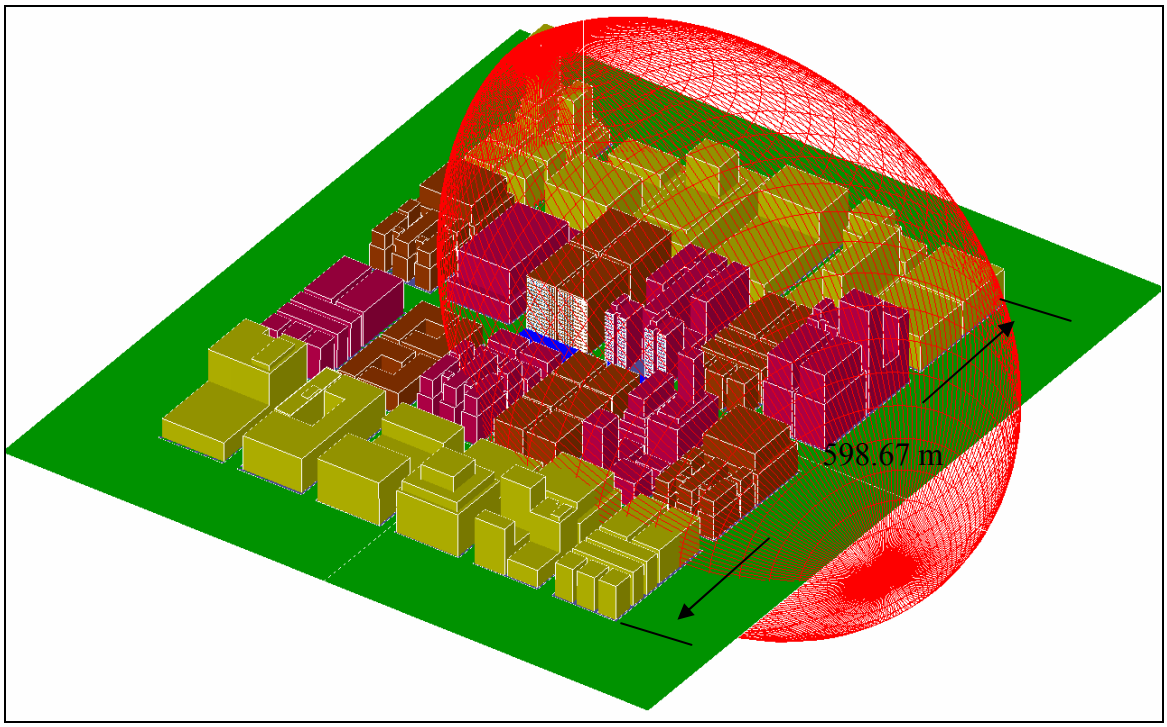

Figure 18. Antenna 1 pattern

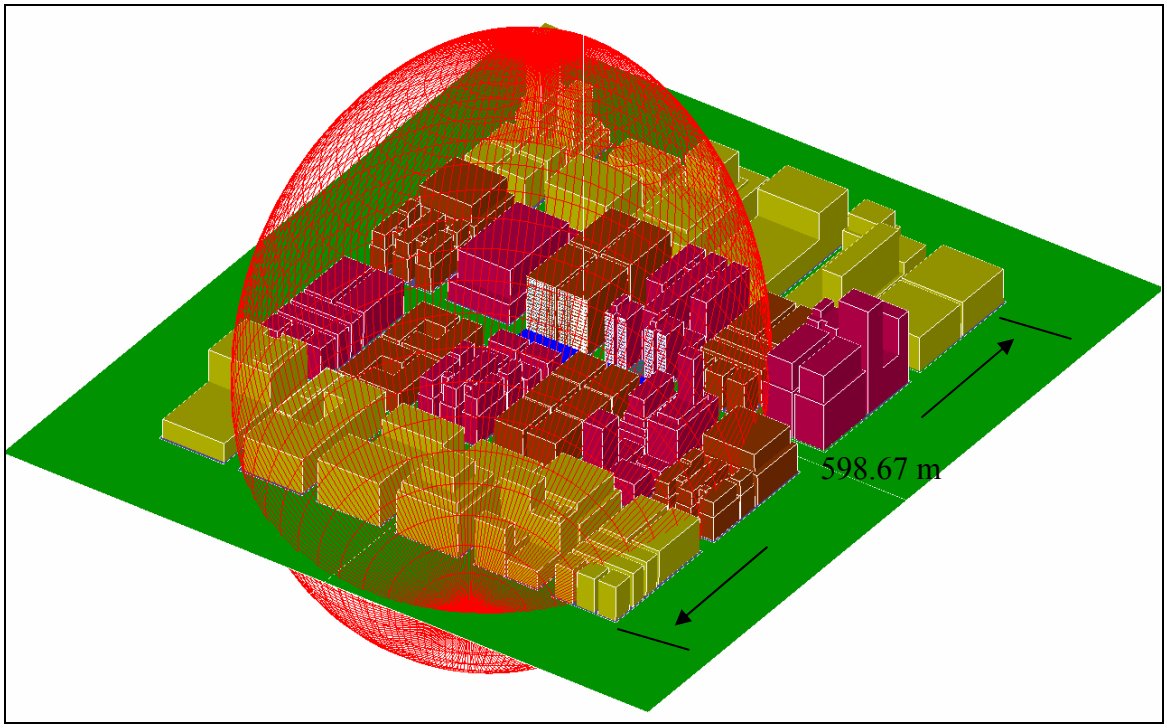

Figure 19. Antenna 2 pattern

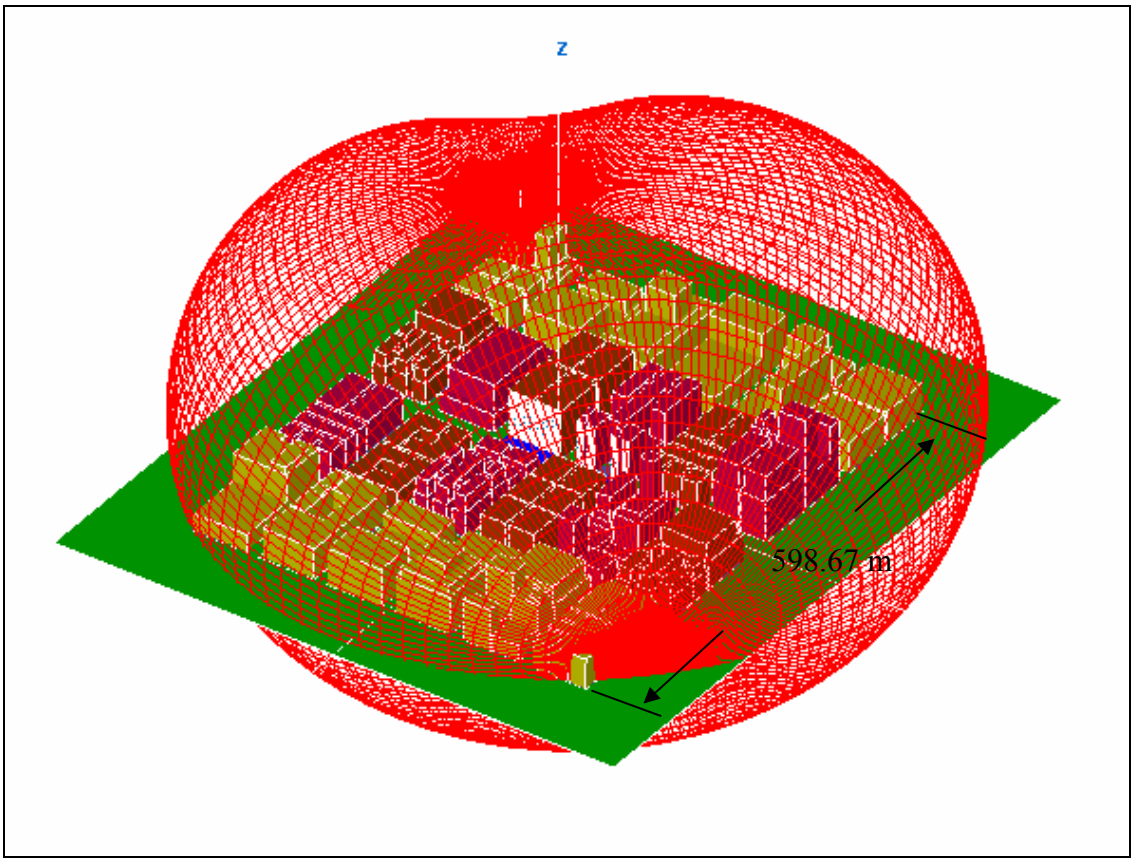

Figure 20. Antenna 3 pattern

B. SIMULATION RESULTS FOR BUILDING MATERIALS

The goal of the first objective was to investigate the effect of details, such as the windows of high-rise buildings, on the radiowave propagation in the dense urban environment. In order to satisfy this objective, a set of reference data must be established. This is accomplished by performing a simulation with the baseline model that lacks the details. The simulation was then repeated with a more detailed test model. These simulations were performed with identical set up for all parameters. After the data was collected, an analysis was performed to determine the difference in signal levels between these models. Table 4 presents the results from the simulations where materials and test conditions were kept constant. Only the reflected and diffracted fields were considered.

Table 4. Simulation results of the diffracted and reflected fields for concrete buildings

Building Material	Test Freq. (MHz)	Ant	Sample Size	Baseline model (dBm)			Detailed model (dBm)			Delta
				Avg.	Std.	Max.	Avg.	Std.	Max.	
CONCRETE	850	1	23410	-56.61	2.30	-42.67	-55.91	1.59	-41.36	0.71
		2	23410	-55.86	3.16	-41.07	-57.61	4.92	-41.40	-1.75
		3	23410	-55.26	2.34	-40.44	-56.74	3.82	-41.86	-1.48
	900	1	23410	-57.02	1.89	-44.00	-56.23	1.09	-41.47	0.79
		2	23410	-55.92	3.23	-41.82	-56.84	4.15	-41.57	-0.92
		3	23410	-55.42	1.69	-44.56	-55.86	2.14	-40.54	-0.45

The column "Avg." is the average power over all cells in the observation grid for an isotropic receive antenna. The overall average value of the baseline model is consistent with the range of the values in detailed model. These values are well above the typical receiver's threshold detection (-90 dBm), therefore this difference will not have a significant impact on the receiver's signal at the observation area.

The building material was changed from concrete to simple perfect electrically conducting (PEC) material, and the simulations were repeated. The results for PEC buildings are shown in Table 5. The all PEC buildings model is not realistic, but it served as a reference for comparison. The overall average is about 10 dBm higher for buildings with PEC material than the buildings with concrete material.

The magnitude difference between the baseline and detailed models shown in the column labeled "Delta" in Table 5 is small. This implies that the number of windows that were used in these simulations did not, on average, have significant effect on radiowave propagation in the observation area. These results also show that changing frequency from 850 MHz to 900 MHz did not have a significant effect for either material.

Table 5. Simulation results of the diffracted and reflected fields for PEC buildings

Building Material	Freq. (MHz)	Ant	Sample Size	Baseline model (dBm)			Detailed model (dBm)			Delta
				Avg.	Std.	Max.	Avg.	Std.	Max.	
PEC METAL	850	1	23410	-48.01	2.38	-33.74	-48.49	2.85	-33.79	-0.48
		2	23410	-47.17	2.57	-32.51	-46.65	2.05	-32.47	0.53
		3	23410	-45.20	1.94	-32.97	-45.60	2.34	-32.62	-0.40
	900	1	23410	-48.63	2.45	-35.79	-48.76	2.59	-35.47	-0.13
		2	23410	-47.72	2.53	-34.30	-47.34	2.15	-34.32	0.39
		3	23410	-45.68	3.15	-32.81	-45.07	2.54	-31.29	0.61

Figures 21 through 32 are the graphical representations of the delta signal contours. Each figure presents a simulation condition, and these conditions are summarized in Table 6. The upper and lower limits of values displayed in each figure are given in the color bars by the numbers on the right hand side.

Table 6. Summarized simulation parameters

Figure number	Antenna	Building material	Frequency (MHz)
Figure 21	1	Concrete	850
Figure 22	2	Concrete	850
Figure 23	3	Concrete	850
Figure 24	1	Concrete	850
Figure 25	2	Concrete	850
Figure 26	3	Concrete	850
Figure 27	1	PEC	900
Figure 28	2	PEC	900
Figure 29	3	PEC	900
Figure 30	1	PEC	900
Figure 31	2	PEC	900
Figure 32	3	PEC	900

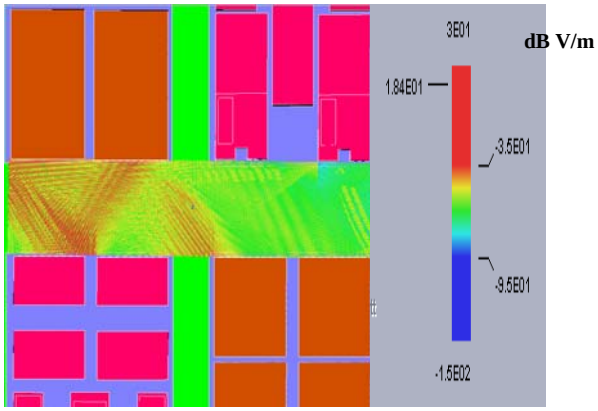

Figure 21. Signal difference between baseline and detailed models for antenna 1 and concrete buildings f = 850 MHz

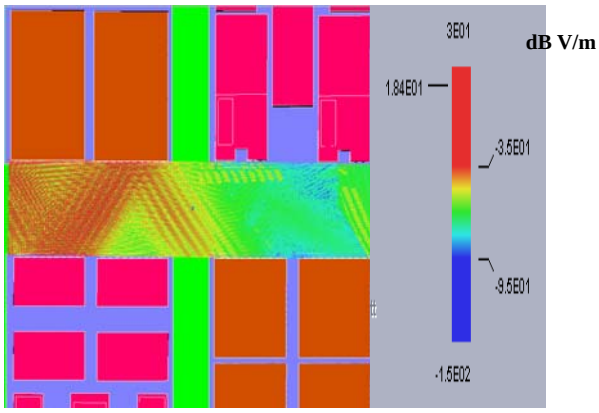

Figure 22. Signal difference between baseline and detailed models for antenna 2 and concrete buildings f = 850 MHz

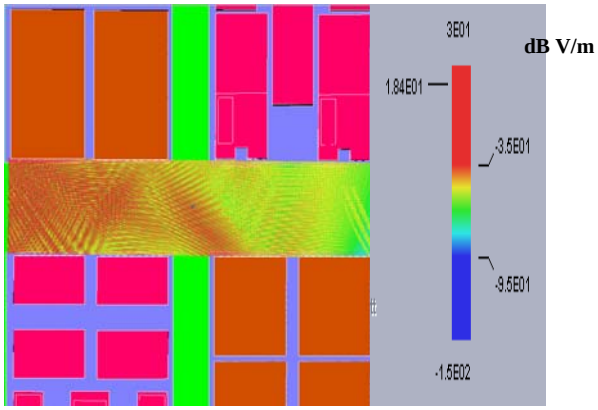

Figure 23. Signal difference between baseline and detailed models for antenna 3 and concrete buildings f = 850 MHz

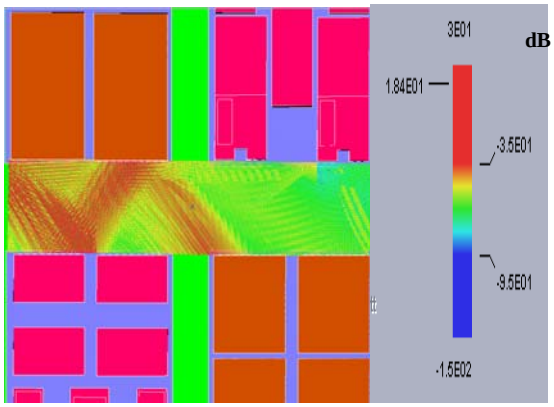

Figure 24. Signal difference between baseline and detailed models for antenna 1 and concrete buildings f = 900 MHz

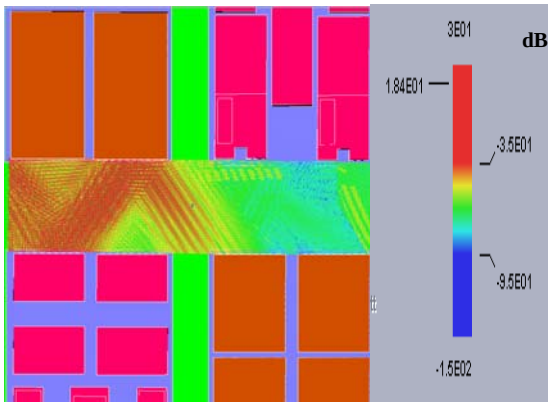

Figure 25. Signal difference between baseline and detailed models for antenna 2 and concrete buildings f = 900 MHz

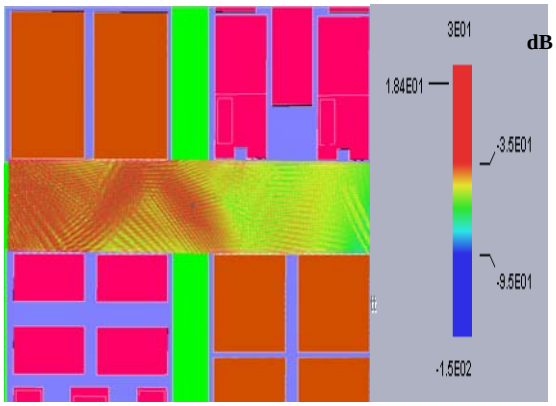

Figure 26. Signal Difference between baseline and detailed models for antenna 3 and concrete buildings f = 900 MHz

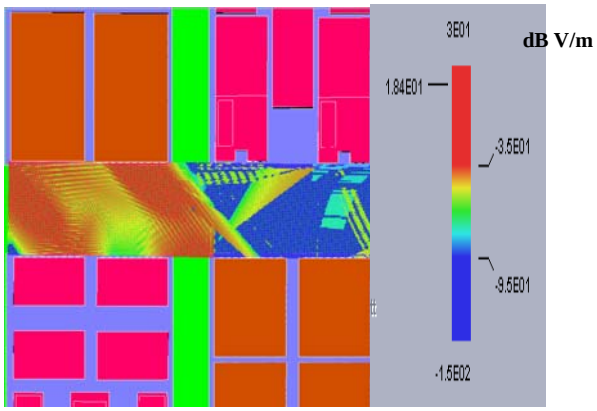

Figure 27. Signal difference between baseline and detailed models for antenna 1 and PEC buildings f = 850 MHz

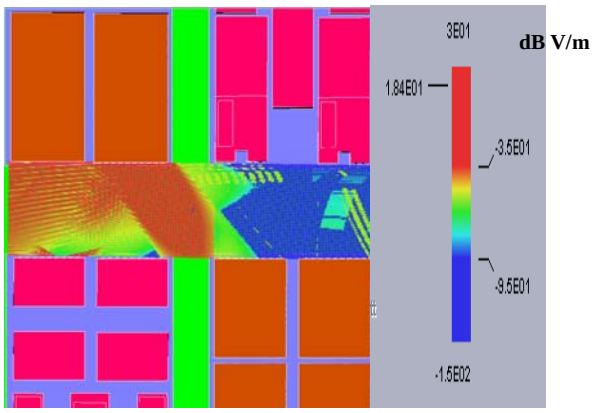

Figure 28. Signal difference between baseline and detailed models for antenna 2 and PEC buildings f = 850 MHz

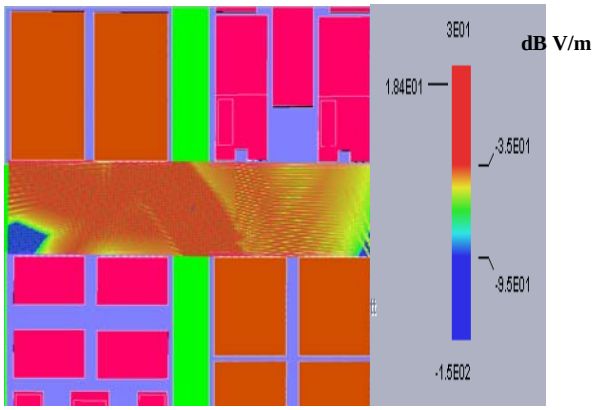

Figure 29. Signal difference between baseline and detailed models for antenna 3 and PEC buildings f = 850 MHz

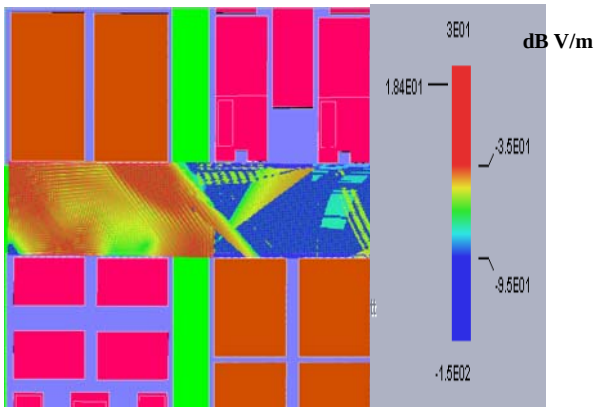

Figure 30. Signal difference between baseline and detailed models for antenna 1 and PEC buildings $f = 900$ MHz

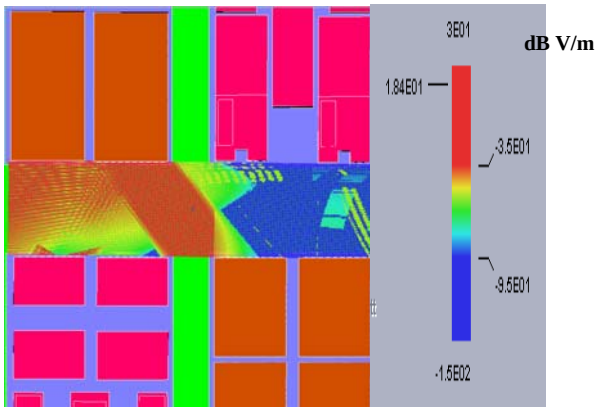

Figure 31. Signal difference between baseline and detailed models for antenna 2 and PEC buildings $f = 900$ MHz

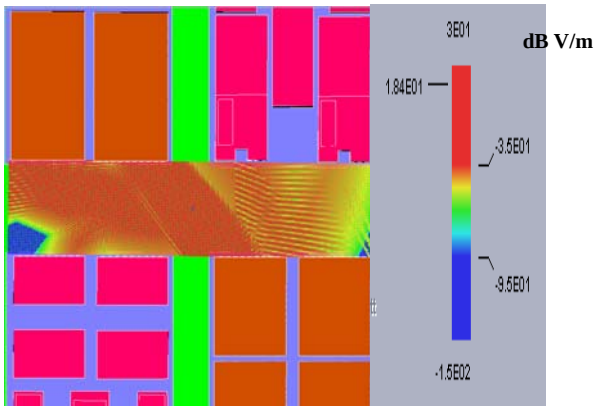

Figure 32. Signal difference between baseline and detailed models for antenna 3 and PEC buildings $f = 900$ MHz

Figures 33 and 34 show the signal contours of a simulation for the entire model area. These figures also illustrate some effect of the individual components of ray tracing. A vertical dipole was used as the transmit antenna.

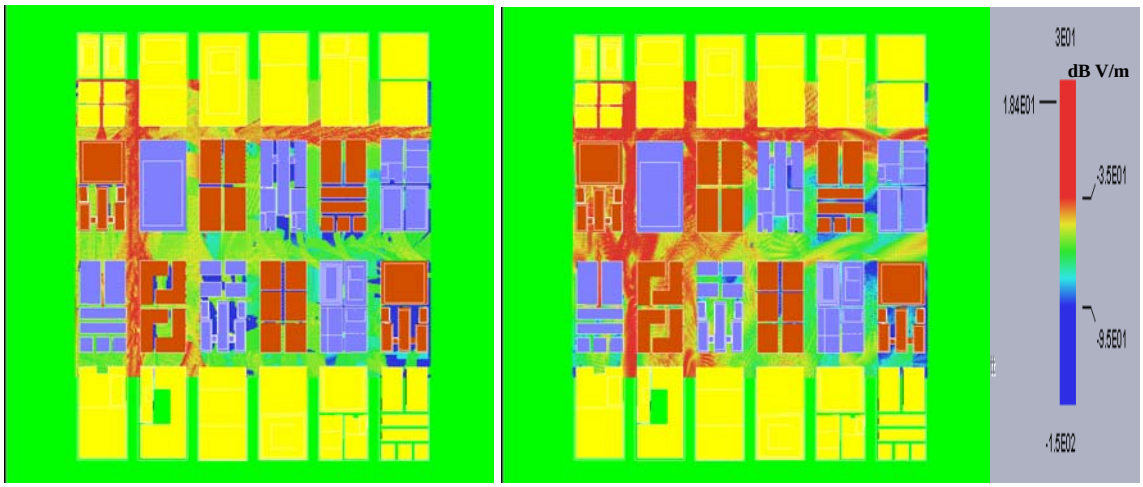

(a) (b)

Figure 33. Simulation of an entire area with antenna 3 (a) diffracted fields (b) reflected fields

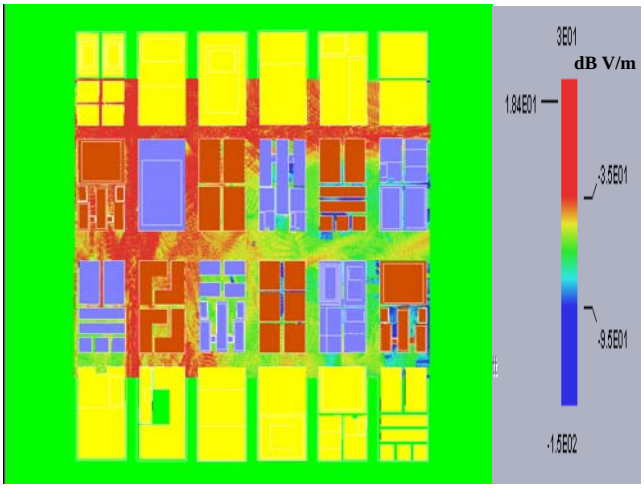

Figure 34. Simulation of an entire area for total field with antenna 3 (incident, reflected, and diffracted fields)

Results from these simulations show that it is not necessary to build a model to the level of detail such as adding windows. Even though the signal contours show some variation of reflections around the area of the windows, it is not high enough to be considered significant. Therefore details of modeling should be focus somewhere else, such as billboards, and street signs.

C. SIMULATION RESULTS FOR ANTENNA PATTERNS

Next, we examine how the base station properties (the antenna gain, half power beamwidth, location, and pointing angle) affect the coverage. A series of simulations was conducted in support of this objective. Table 7 contains results from these simulations. In this case the total fields were used, because they are the actual signals available to a mobile user.

Table 7. Simulation results of the total fields for detailed model

Material	Freq. (MHz)	Sample Size	Combine Ant 1 & 2 (dBm)			Ant 3 (dBm)			Delta
			Avg.	Std.	Max.	Avg.	Std.	Max.	
CONCRETE	850	23410	-53.22	2.66	-38.22	-56.74	3.63	-41.86	3.52
	900	23410	-53.34	3.02	-38.56	-55.86	4.27	-40.54	2.52
PEC	850	23410	-44.25	2.86	-29.49	-45.6	2.14	-32.62	1.35
	900	23410	-44.67	2.32	-30.72	-45.07	3.07	-31.29	0.4

In this simulation, antenna 1 and antenna 2 transmitted separately, and their fields were combined to obtain the sum of the signal strength at each point in the observation grid. The procedure used was first to establish an effective radiated power (ERP) that is equal for both antennas under consideration. Therefore it was necessary to compute a transmitter power, P_t, for each antenna used in these simulations that would produce the desired ERP. See Chapter II Section C for details.

For antennas 1 and 2 the transmit power is 1 W (30 dBm) into each antenna. A similar calculation was done to compute P_t for antenna 3 that would yield the same ERP, which was found to 34.8 dBm.

The data in Table 7 is based on both antennas 1 and 2 transmitting simultaneously each with the full transmitting power. The average power of the combined antennas 1 and 2 is greater than the average value of the antenna 3, as expected.

The results from these simulations demonstrated that it is not necessary to focus on the details of modeling and simulation, or the number of antennas needed for the simulation process. The average values over the observation grid are relatively

insensitive to these things. Perhaps attention should focus more on billboards, signal signs, parked cars, or some other objects that could cause higher reflection.

The following chapter presents the conclusions for this thesis and offers a few topics for possible future work.

THIS PAGE INTENTIONALLY LEFT BLANK

IV. CONCLUSIONS AND FUTURE WORK

A. SUMMARY

One objective of this thesis was to investigate the effect of details, such as the windows of high-rise buildings, on the radiowave propagation in the dense urban environment. A second objective was to investigate base station antenna coverage, that is, the antenna gain, half power beamwidth (HPBW), location, and pointing angle to give the maximum coverage over a specified sector.

The buildings were adapted from an existing CAD model of NYC, Manhattan Island. Each building was then reshaped and resized to match the dimensions of the actual city blocks. Two models were built for comparison. The two models were identical in size, number of buildings, and building materials. Only one of these models has windows. The other model is used as a baseline for comparison.

Urbana Wireless Toolset was the primary software used for simulations. It is generally assumed that detailed modeling of the buildings and it environment are required for an accurate prediction of the signal contours since the signal contour prediction by *Urbana* will only be as good as the accuracy of the information provided. *Urbana* does not take into account the mobility of objects in the models and natural attenuation due to atmospheric conditions like rain and fog. After the simulations were completed, *Matlab* and *Microsoft Excel* were used to analyze data and display tabular results. However, the field strength contour plots were generated by *Urbana.*

Typical cell phone frequencies of 850 MHz and 900 MHz were selected for this research. Several other input parameters were also varied in the process of simulation, such as, building material, observation areas, transmitting power, and antenna patterns, to obtain sufficient data to satisfy the objectives for this research.

B. CONCLUSIONS

The results and data analysis from the simulation have shown that varying frequency over the specified range did not show significant impact on the overall results. However, the building material can contribute some impact on the signal propagating in the environment. The average power for buildings with PEC material is consistently higher by 9 dBm in comparing to the case of buildings with concrete material. This was primarily due to the fact that the location of the observation grid happened to be in an area of strong reflections. Materials that have higher transmission coefficients result in more diffuse signal distribution.

Based on the simulation results and data shown in Table 4, we can conclude that adding windows will not significantly change the signal distribution on average. It is important to emphasize that this statement applies to average values over the observation grid. There are some points that increase or decrease substantially, but taken on the average, the levels remain about the same. Therefore it may not be necessary to build a detailed model with the correct building material in order to obtain good results from the simulations.

The second objective was to determine which antenna options would provide the maximum coverage over a specified sector. The results from these simulations and data shown in Table 7 indicate that it is no more advantageous to utilize two antennas with lower transmitting power and higher antenna gain than a single wider beamwidth antenna that uses a higher transmitting power.

C. FUTURE WORK

A more detailed profiling of an urban environment such as in downtown Los Angeles would be useful. Model details should include billboards, lamp posts, street signs, trees, and parked cars to fully assess their impact on simulation results.

Future work can also include validation and verification of the simulation results through actual measurements.

Multiple diffraction should be investigated. Unfortunately *Urbana* only does "over the roof" diffraction (not multiple diffraction from vertical edges). Reference [4] indicates that multiple diffraction from vertical edges can be significant.

THIS PAGE INTENTIONALLY LEFT BLANK

LIST OF REFERENCES

[1] Ghoraish, M., *"*Identification of scattering objects in microcell urban mobile propagation channel,*" IEEE Transactions on Antennas and Propagation*, Vol. 54, No. 11, November 2006.

[2] De Jong, Y. and Herben, M., *"*A tree scattering model for improved propagation prediction in urban microcells*," IEEE Transactions Veh. Technol.*, Vol. 53, No. 2, pp. 503-513, March 2004.

[3] Thomas, N. J., Willis, M. J., Graig. K. H., *"*The relative importance of different propagation mechanisms for radio coverage and interference prediction in urban scenario at 2.4, 5.8, and 28 GHz,*" IEEE Transactions on Antennas and Propagation.*, Vol. 54, No. 12, March 2004.

[4] Dimitriou, A. G., and Sergiadis, G. D., *"*Architectural features and urban propagation*," IEEE Transactions on Antennas and Propagation.*, Vol. 54, No. 3, March 2006.

[5] Poh, C. S., *"*Simulations of diversity techniques for urban UAV data links,*"* Master's Thesis, Naval Postgraduate School, Monterey, December 2004.

[6] Pala, F., "Frequency and polarization diversity simulations for urban UAV Communication and Data Links," Master's Thesis, Naval Postgraduate School, Monterey, September 2004.

[7] http://inetours.com/New_Orleans/images/Blcny/Balcony1.jpg, last accessed March 2007.

[8] http://www.multi-housingnews.com, last accessed March 2007.

[9] Ulaby, T. F., *Fundamentals of Applied Electromagnetics,* Media Edition, Prentice Hall Upper Saddle River, New Jersey, 2004.

[10] Wikipedia web site, http://en.wikipedia.org, last accessed February 2007.

[11] Jenn, D. C., *Lecture Notes for EC3630 (Radiowave Propagation)*, Naval Postgraduate School, 2006 (unpublished).

[12] Stutzman, L. W., and Thiele, A. G., *Antenna Theory and Design,* 2nd Edition, John Wiley & Sons Inc., Hoboken, NJ 07030, 1998.

[13] Siwiak, K., *Radiowave Propagation and Antennas for Personal Communications,* 2nd Edition, Artech House, Inc., Norwood, Massachusetts, 1998.

[14] Walfisch, J., and Bertoni, H., "A theoretical model of UHF propagation in urban environments," *IEEE Trans. Antennas and Propagate*, Vol. 36, pp. 1788– 1796, December 1988.

[15] Crosby, D., Creaves, S., and Hopper, A.," The effect of building height variation on the multiple diffraction loss component of the Walfisch-Bertoni model," *IEEE Personal, Indoor and Mobile Radio Communications*., Vol. 2, pp. 1805-1809, Sept. 2003.

[16] Hata, M., "Empirical formula for propagation loss in land mobile radio services," *IEEE Transactions on Vehicular Technology*, Vol. VT-29, No. 3, 1980.

[17] *Urbana* 3-D Wireless Toolkit, http://www.saic.com/products/software/urbana/, last accessed July 2006.

INITIAL DISTRIBUTION LIST

1. Defense Technical Information Center
   Ft. Belvoir, Virginia

2. Dudley Knox Library
   Naval Postgraduate School
   Monterey, California

3. Chairman,
   Department of Electrical and Computer Engineering
   Naval Postgraduate School
   Monterey, California

4. Professor David C. Jenn
   Department of Electrical and Computer Engineering
   Naval Postgraduate School
   Monterey, California

5. Professor Donald Z. Wadsworth
   Department of Electrical and Computer Engineering
   Naval Postgraduate School
   Monterey, California

6. Pete Burke
   Building 1030 NT, Rm 211
   Edwards AFB, CA

7. Chris Chung
   Lancaster, California